Journal of the Mechanics and Physics of Solids 56 (2008) 1320–1347

JOURNAL OF THE
MECHANICS AND
PHYSICS OF SOLIDS

A micromorphic model for the multiple scale failure of

in the form of grains, fibers or different size particles. In this work, we propose to use the multi-scale micromorphic theory (

2. Multi-scale model

2.1. Ductile fracture mechanisms

In the study of ductile fracture mechanisms, the distinct role of primary and secondary particles can be deduced by observation of the fracture surface. Because bonding at the particle–matrix interface is stronger

2.2. Multi-scale decomposition of the microstructure

As noted above, ductile fracture in high strength steel alloys is a highly nonlinear phenomenon that encompasses several mechanisms across three scales: macro-scale, scale of primary particles, and scale of secondary particles. Following Vernerey et al. (2007) it is possible to associate to each scale of analysis an independent kinematic variable, arising from the introduction of material domains centered on a material point x. The three kinematic variables and the associated nested domains shown in Fig. 2 are defined as follows:

the macro-velocity v

homogenization techniques (Nemat-Nasser and Hori, 1999

Note that this operation introduces length scales $\bar{\ell}^1$ and $\bar{\ell}^2$ in the model and can be interpreted through Eq. (6) as a measure of the lever arm of the stress couples.

3.2. Elastic response

In this study, an additive decomposition of the generalized rate of deformation into an elastic part $\mathbf{\Delta}^e$ and a plastic part

In the following, we present a derivation of the yield function and an evolution of internal variables associated with each scale, starting at the macro-scale. While the macroscopic plastic response is determined based on hierarchical homogenization techniques described in Hao et al. (2004), the microscopic and submicroscopic constitutive relations remain empirical but physically motivated.

Note that although the material's microstructure is typically anisotropic and discontinuous at small scales,

eqsy

where b_{vs} is a function of the debonding stress s^s. At the onset of a void-sheet mechanism, micro-stresses lie on the yield surface, implying that $F^1 = 0$. Using Eqs. (20) and (A.16), we can write

$$B^1_{y0} = (B^1_{eq} + aB^1_m)|_{f + a_{vs}\varepsilon_p = b_{vs}}. \tag{21}$$

For simplicity, we assume that B^1_y is a linear function of E^1

$$B^1_y = B^1_{y0}(1 + h^1 E^1). \tag{22}$$

The coefficient h^1 remains an arbitrary constant and gives the sensitivity of micro-stress softening with the amount of micro-deformation. Computations have shown that the behavior of the solution exhibits insignificant variations when we modify the value of h^1. In the following, we consider perfect plasticity for the inhomogeneous response at the micro-scale; in other words, we choose $h^1 = 0$.

3.3.3. Submicroscopic plastic response

The submicro-stress and submicro-stress couples are a result of inhomogeneous stresses induced by microvoid growth. At this scale, plastic instability occurs when the matrix material fails to carry stress moments after the onset of microvoid coalescence (or instability of ligaments between microvoids). Submicroscopic plastic deformation can subsequently be defined as the plastic deformation of the matrix material after the onset of void coalescence (necking of ligament). The yield function is written in the form of J_2 flow plasticity modified to account for the effects of higher order stresses:

$$F^2(\bar{\boldsymbol{\beta}}^2, \bar{\bar{\boldsymbol{\beta}}}^2, Q) = B^2_{eq} \quad B^2_y = 0, \tag{23}$$

where B^2_{eq} is the overall equivalent micro-stress and B^2_y is the micro-yield stress. The equivalent stress and rate of plastic micro-strain E^2 are written in the form:

$$B^2_{eq} = \quad \frac{3}{2}\bar{\boldsymbol{\beta}}^{2,dev} \quad \bar{\boldsymbol{\beta}}^{2,dev} + \left(\frac{a^1}{\ell^1}\right)^2 \bar{\bar{\boldsymbol{\beta}}}^{2,dev} \quad \bar{\bar{\boldsymbol{\beta}}}^{2,dev},$$

$$E^2 = \quad \frac{2}{3}(D^{2,p} \quad D^p) \quad (D^{2,p} \quad D^p) + b^2\bar{\ell}^2 D^{2,p} \quad \overset{!}{r}$$

techniques. One of the critical feature to capture from cell modeling is the strength of the interface between particles and matrix material. For this, we used the cohesive model described next.

3.4.1. Matrix/particles cohesive law

The interfacial debonding energy at Fe–TiC interface for secondary particles and Fe–TiN interface for

3.4.2. Hierarchical homogenization

The hierarchical framework used in this study is depicted in Fig. 6. Homogenization of the material at the level of secondary particles is first carried out to produce a homogenized constitutive relation that can be used to model the material between primary particles. A cell model at the scale of primary particles is then used to determine properties of the material at the macro-scale. At each scale, we introduce a representative cell O in plastic potential F' (Gurson, 1977) with adjustable parameters as follows:

$$F' = \left(\frac{\sigma'_{eq}}{\sigma_y}\right)^2 + 2q'_1 f' \cosh\left(\frac{3q'_2\sigma'_m}{2\sigma_y}\right) \quad (1 + q'_3(f')^2) = 0, \tag{29}$$

where the prime denotes the scale of secondary particles. Here, σ'_m is the hydrostatic stress and σ'_{eq} is the equivalent stress. The determination of constants q'_1, q'_1 and q'_1 is described in Appendix C. The evolution of the microvoid volume fraction f' is decomposed into a nucleation term, growth term and coalescence term. The evolution of each of these internal variables is described in Appendix A.1. Note that the function F' is only used temporary in order to determine the macroscopic material response. It is not used in the multi-scale framework described in previous sections.

The macroscale yield function is then determined by considering the unit cell containing a distribution of randomly distributed primary particles in a matrix whose response is given by Eq. (29). A similar averaging operation is performed to lead to the form of the yield function (12) and the evolution of internal variables given in Eq. (14).

4. Implemented multi-scale model results

4.1. One-dimensional analysis

The behavior of the three-scale micromorphic steel model is first investigated in a simple one-dimensional

4.1.1. Three-scale continuum solution

In Fig. 8, the evolution of the profile of macroscopic logarithmic tensile strain is plotted as a function of position along the bar. Each of the three distinct stages is observed in failure of the bar based on the size of the corresponding localization region.

Stage 1 corresponds to localization of the deformation as a result of macroscopic material instability (due to the nucleation of voids from primary particles in the center of the bar). The width of the localization zone is due to micro- and micro-stress couple that are associated with the length scale $\bar{\ell}^1$.

Stage 2 corresponds to the second level of localization, associated with microscopic instability. At this stage, due to sufficient plastic strains and voids growth around the primary particles, microvoid nucleation

Two computations are performed. First, a direct numerical simulation (DNS) of the shear test with explicit modeling of two populations of particles and second, a computation of the equivalent three-scale

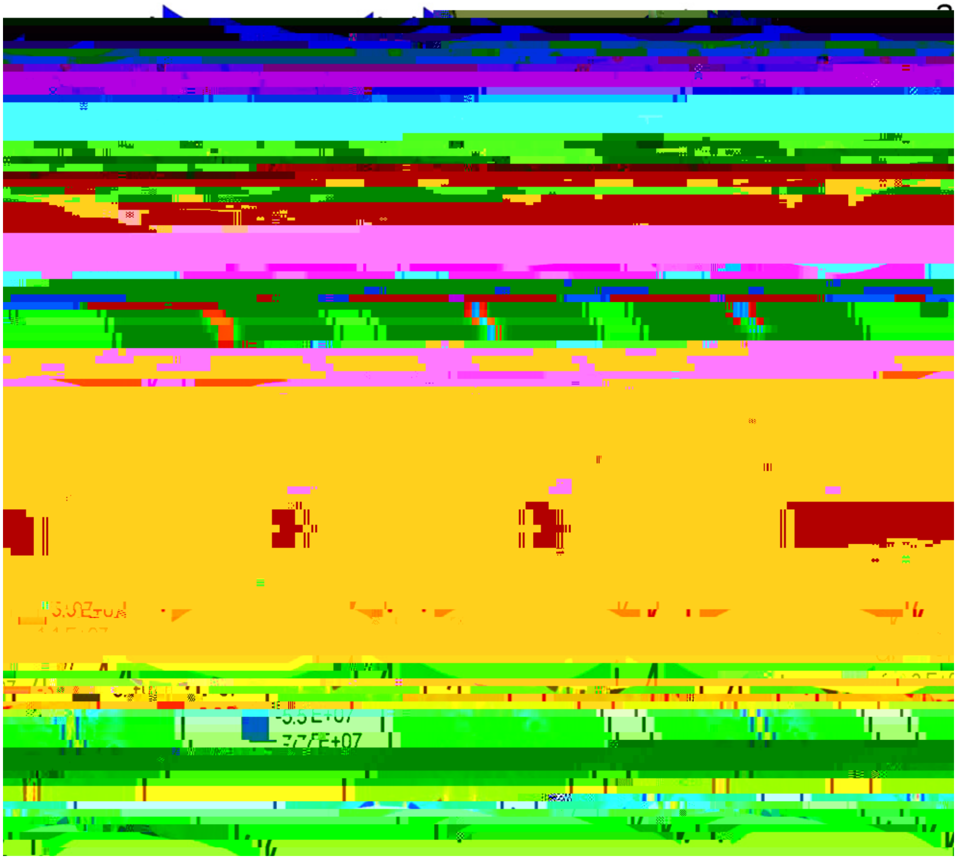

Fig. 12. (a) Snapshots of the plastic deformation of the shear specimen with explicit microstructure; (b–d) snapshots of the plastic

The evolution of effective plastic strains at macro-, micro- and submicro-scales are depicted in Fig. 15 for different times. Three stages of material failure are shown. The first stage corresponds to material instability at

Acknowledgments

where B'_1 represents the acceleration of void growth in high triaxiality and B'_2 was added to represent the shear driven void coalescence such that:

$$\begin{array}{lll} B'_1 = 0, & B'_2 = 0 & \text{before the onset of coalescence,} \\ B'_1 > 0, & B'_2 > 0 & \text{after the onset of coalescence.} \end{array} \tag{A.9}$$

Cell modeling studies showed that the criterion for the onset of void coalescence can be expressed as follows:

$$f' + a_c \varepsilon'_p - b_c > 0, \tag{A.10}$$

where $a_c = 0.1222$ and $b_c = -0.1236$. In other words, coalescence takes place either at high void volume fraction or at high plastic strains. The trade-off between those quantities is given by the relation (A.10).

A.2. Homogenization at the scale of primary particles

The macroscopic yield function is written in the form:

$$F = \left(\frac{\sigma_{eq}}{\sigma_y}\right)^2 - 1 + 2q_1\left(f^P + f^S\right)\cosh\left(\frac{3q_2\sigma_m}{2\sigma_y}\right) - q_3\left(f^P + f^S\right)^2 = 0. \tag{A.11}$$

The evolutions of void volume fraction nucleating from primary and secondary particles are taken in the following form:

$$f^P = f^n + f^g \text{ and } f^S = f^c. \tag{A.12}$$

The first term f^n denotes the nucleation of voids around primary particles, the second f^g represents the growth of those voids under the action of hydrostatic stress and finally, f^c is the coalescence term. The coalescence stage can be explained with the void-sheet mechanism (Horstemeyer et al., 2000) as follows: as larger voids grow, the plastic strain in the matrix material increase significantly, leading to nucleation of the smaller population of voids. The newly nucleated microvoids are then free to grow and coalesce in the sheet driven coalescence is on the straight line given by

$$f + a_{vs}\varepsilon_p \quad b_{vs}(s^S) = 0, \tag{A.16}$$

where $a_{vs} = 0.0639$ and b_{vs} is a linear function of the debonding stress (in GPa):

$$b_{vs}(s^S) = (0.0043s^S + 0.0186). \tag{A.17}$$

Eqs. (A.16) and (A.17) can be interpreted as follows. Void-sheet coalescence occurs either in high volume fraction and low plastic strain or in high plastic strain and low volume fraction. This can be explained by the fact that both an increase of volume fraction and plastic strain have a direct influence on the strains between larger voids. Finally, a stronger interface at the secondary particle/matrix, by postponing small void nucleation, has the effect of delaying the coalescence.

Appendix B. Material models

B.1. Material constants for Von-Mises model

The derivation of material constants of the generalized Von-Mises plasticity model is similar to the Drucker–Prager model presented in Section B.2 by setting $a = 0$.

B.2. Material constants for Drucker–Prager model

In this appendix, we show the derivation of material constants for the generalized Druker–Prager model utilized for the constitutive relation at the microscale. Let us first develop an expression for the averaged deviatoric and volumetric stresses $\bar{\boldsymbol{\beta}}^{1,\mathrm{dev}}$, $\bar{}$

where the constant c^1 ¼ 1/18. Extending the idea of de Borst (1993) for the Druker–Prager model, the material constants a^1 and b^1 are now determined based on the equality of the plastic multiplier and the equivalent plastic strain:

$$E^1 \text{ ¼ } l^1 \quad 1 \text{ þ } 2a^2. \tag{B.6}$$

Let us first write the plastic flow directions $\bar{r}^1$ and $\bar{\bar{r}}^1$ as follows:

$$\bar{r}^1_{ij} \text{ ¼ } \frac{\partial F^1}{\partial \bar{b}^{1,\mathrm{dev}}_{ij}} \text{ ¼ } \frac{3}{2}\frac{}{}\,{,}1\mathrm{dev}$$

u_1^T and u_2^T are the displacements of the nodes on the top boundary in the y_1 and y_2 directions, respectively.
u_1^B and u_2^B are the displacements of the nodes on the bottom boundary in the y_1 and y_2 directions, respectively.

In order to apply the periodic boundary conditions, let us introduce two dummy nodes N' and N'' of respective displacements u' and u''. The displacements of nodes on the boundaries of the RVE are then constrained as follows:

$$\begin{aligned} u_1^R - u_1^L &= u_1', \\ u_2^T - u_2^B &= u_2', \\ u_1^T - u_1^B &= u_1'', \\ u_2^R - u_2^L &= u_2''. \end{aligned} \tag{C.1}$$

This can be done in the commercial software ABAQUS© by using the linear constraint option. With those constraints, only the four boundary conditions on the dummy node need to be prescribed and the average true strain in the RVE is then given by the following relation:

$$\begin{bmatrix} \varepsilon_{11} & \varepsilon_{12} \\ \varepsilon_{21} & \varepsilon_{22} \end{bmatrix} = \begin{bmatrix} \log\left(1 + \dfrac{u_1'}{D_1}\right) & \log\left(1 + \dfrac{u_1''}{D_2}\right) \\ \log\left(1 + \dfrac{u_2''}{D_1}\right) & \log\left(1 + \dfrac{u_2'}{D_2}\right) \end{bmatrix}. \tag{C.2}$$

Moreover, the linear constraint implies that the total reaction forces on the boundaries of the RVE are the forces f' and f'' on the dummy nodes. The average Cauchy stress in the RVE defined as the boundary traction per unit area is therefore written as follows:

$$\begin{bmatrix} s_{11} & s_{12} \\ s_{21} & s_{22} \end{bmatrix} = \begin{bmatrix} \dfrac{t_1'}{D_2 + u_2'} & \dfrac{t_1''}{D_1 + u_1'} \\ \dfrac{t_2''}{D_2 + u_2'} & \dfrac{t_2'}{D_1 + u_1'} \end{bmatrix}. \tag{C.3}$$

C.2. Constant stress ratio with periodic BC

This is done via the definition of a user-element in ABAQUS© (subroutine UEL) and the subroutine DLOAD.

The procedure consists of computing the average stress s_{22} during the simulation and applying the pressure p on the sides such that we have:

$$p ¼ Rs_{22}. \tag{C.4}$$

However, as the RVE is displacement controlled, the stress s_{22} is not explicitly known during the simulation and must be determined through a special procedure. The latter consists in defining a user element subroutine that computes the stress s_{22} at each time step and pass it to the subroutine DLOAD that applies the resulting pressure p on the left and right boundaries.

Referring to Fig. 17, we first introduce an additional dummy node N, located straight above node N^{0} such that the user element consists of two nodes and three degree of freedom as follows:

the displacement u_2 of node N;
the displacements u^{0}_1 and u^{0}_2 of node N^{0}.

The procedure consists of applying the vertical displacement boundary condition on node N instead of N^{0} and linking the two nodes with a stiff spring of stiffness K. The tensile force t^{0}_2 on node N^{0} is therefore given by

$$t^{0}_2 ¼ Kðu_2 \quad u^{0}_2þ. \tag{C.5}$$

It is then straightforward to obtain the stress s_{22} with the knowledge of u^{0}_1,

$$s_{22} ¼ \frac{t^{0}_2}{D_1 þ u^{0}_1} ¼ \frac{Kðu_2}{}$$

References

Bazant, Z., Jirasek, M., 2002. Nonlocal integral formulations of plasticity and damage: survey of progress. J. Eng. Mech. 128, 1119–1149.

Cowie, J.G., Azrin, M., Olson, G.B., 1989. Microvoid formation during shear deformation of ultrahigh strength steels. Metall. Trans. 20A, 143–153.

de Borst, R., 1993. A generalization of j2-flow theory for polar continua. Comput. Methods Appl. Mech. Eng. 103, 347–362.